

See discussions, stats, and author profiles for this publication at: <https://www.researchgate.net/publication/231648430>

Crystal Plane-Dependent Compositional and Structural Evolution of Uniform Cu₂O Nanocrystals in Aqueous Ammonia Solutions

ARTICLE in THE JOURNAL OF PHYSICAL CHEMISTRY C · OCTOBER 2011

Impact Factor: 4.77 · DOI: 10.1021/jp206966f

CITATIONS

33

READS

72

5 AUTHORS, INCLUDING:



[Qing Hua](#)

University of Science and Technology of China

22 PUBLICATIONS 503 CITATIONS

[SEE PROFILE](#)



[Kai Chen](#)

University of Science and Technology of China

8 PUBLICATIONS 223 CITATIONS

[SEE PROFILE](#)



[Sujie Chang](#)

University of Science and Technology of China

15 PUBLICATIONS 277 CITATIONS

[SEE PROFILE](#)



[Weixin Huang](#)

University of Science and Technology of China

107 PUBLICATIONS 1,995 CITATIONS

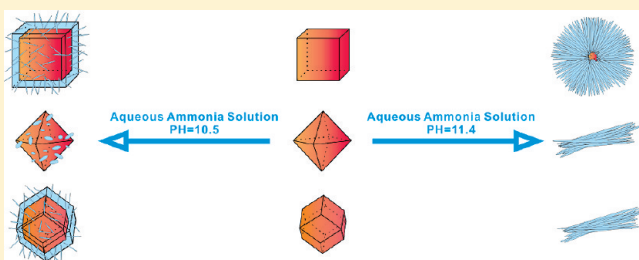
[SEE PROFILE](#)

Crystal Plane-Dependent Compositional and Structural Evolution of Uniform Cu₂O Nanocrystals in Aqueous Ammonia Solutions

Qing Hua,^{†,‡,§} Kai Chen,[†] Sujie Chang,^{†,‡,§} Yunsheng Ma,[§] and Weixin Huang*,^{†,‡,§}

[†]Hefei National Laboratory for Physical Sciences at the Microscale, [‡]CAS Key Laboratory of Materials for Energy Conversion, [§]Department of Chemical Physics, [†]Education Center of Chemical Practice, University of Science and Technology of China, Hefei 230026, China

ABSTRACT: The componential and morphological evolution of uniform Cu₂O nanocrystals with different shapes in aqueous ammonia solutions has been comprehensively studied by means of X-ray diffraction, X-ray photoelectron spectroscopy, scanning electron microscope, and transmission electron microscopy. Cubic, octahedral, and rhombic dodecahedral Cu₂O nanocrystals that, respectively, expose Cu₂O {100}, {111}, and {110} crystal planes exhibit distinctly different reaction behaviors. The stability of various types of uniform Cu₂O nanocrystals in the aqueous ammonia solution follows the order cubic Cu₂O nanocrystals > octahedral Cu₂O nanocrystals > rhombic dodecahedral Cu₂O nanocrystals. The nucleation and growth of Cu(OH)₂ and CuO precipitate also depend on the shape of Cu₂O nanocrystals. The shape-dependent reaction behaviors of Cu₂O nanocrystals were attributed to the type of crystal plane exposed on Cu₂O nanocrystals that determines their surface structure and surface reactivity. Our results well exemplify the crystal plane-dependent reactivity of oxide nanocrystals and greatly deepen our fundamental understanding of complex chemical reactions occurring at the liquid–solid interface.



1. INTRODUCTION

Chemical reactions of solids in solutions are widely involved in many important chemical processes such as electrochemistry, corrosion, reactive dissolution/precipitation, and heterogeneous catalysis. Chemical reactions occurring at the liquid–solid interface always involve the in-situ formation of new solid surface whose structure (composition and morphology) and subsequent reactivity dynamically change; therefore, it is of interest and importance to fundamentally understand the chemical reaction-induced structural evolution of solids in solutions. It is always the surface of solid particles that participates in the liquid–solid interfacial chemical reaction. The surface structure and the composition of an individual solid particle that strongly affect its surface reactivity are determined by the crystal planes exposed on its surface; thus, the investigation of crystal plane-dependent surface reactivity of a solid will greatly facilitate the fundamental understanding of liquid–solid interfacial chemical reactions. However, this has remained as a challenge because of the structural heterogeneousness and complexity of solid particle surfaces. Even an individual solid particle usually exposes several different types of crystal planes with the lowest surface free energies on its surface that all contribute to the observed surface reactivity. The recent progress achieved in the morphology-controlled synthesis of nanocrystals makes it possible to fabricate uniform metal/oxide nanocrystals exclusively exposing one type of crystal plane that provide excellent model systems for the investigation of crystal plane-dependent surface reactivity of a solid.

Cuprous oxide (Cu₂O) is among the oxide nanocrystals whose morphology-controlled synthesis has developed very comprehensively. Numerous Cu₂O nano- and microstructures with well-controlled uniform morphologies have been recently synthesized, including cubes,^{1–3} octahedrons,⁴ {100} truncated octahedrons,⁵ rhombic dodecahedrons,^{6,7} {110} truncated octahedrons,⁶ {100} truncated rhombic dodecahedrons,⁸ 26-facet polyhedral,⁹ nanowires,^{10–13} nanoplates,¹⁴ nanocages,^{15,16} and branched and hollow structures.^{17–20} The structure of as-synthesized Cu₂O nanocrystals has been observed to evolve with their local chemical environment. Park et al.²¹ reported that aqueous ammonia solution could convert Cu₂O nanocubes to polycrystalline CuO hollow nanostructures in air through a sequential dissolution–precipitation process, and increasing the pH value of the solution led to the formation of hollow cubes, hollow spheres, and urchinlike particles. Wang et al.²² reported that uniform hollow structures including Cu₂O@Fe(OH)_x nanorattles with tunable core size and Fe(OH)_x cages could be facilely synthesized by template-engaged redox etching of shape-controlled Cu₂O crystals. Kuo et al.²³ successfully employed cubic and octahedral Cu₂O nanocrystals and Au@-Cu₂O core–shell heterostructures as sacrificial templates to prepare cubic and octahedral Cu₂S nanocages and Au–Cu₂S core–cage structures with thin walls. Wen et al.²⁴ successfully synthesized Cu(OH)₂ nanoribbons that are 20–100 nm

Received: July 21, 2011

Revised: September 13, 2011

Published: September 13, 2011

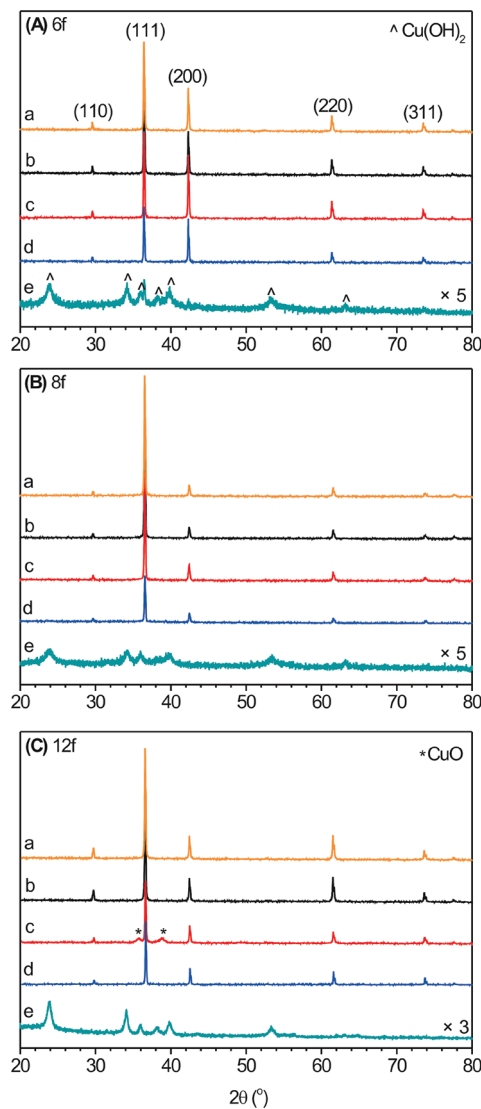


Figure 1. XRD patterns of (A) cubic (6f), (B) octahedral (8f), and (C) rhombic dodecahedral (12f) Cu_2O nanocrystals: (a) as-synthesized Cu_2O nanocrystals; Cu_2O nanocrystals etched in aqueous ammonia solution with $\text{pH} = 10.5$ for (b) 10 min and (c) 150 min; Cu_2O nanocrystals etched in aqueous ammonia solution with $\text{pH} = 11.4$ for (d) 3 min and (e) 40 min.

in width, several nanometers in thickness, and up to $100 \mu\text{m}$ in length by a simple solution-phase process. Siegfried and Choi^{25–27} have systematically investigated the fabrication of Cu_2O nanocrystals and their morphology transformation in an electrochemical environment.

Uniform Cu_2O nanocrystals exclusively exposing one type of crystal plane, including cubes exposing $\{100\}$ crystal planes, octahedra exposing $\{111\}$ crystal planes, and rhombic dodecahedra exposing $\{110\}$ crystal planes, offer a model system for a comprehensive study of crystal plane-dependent surface reactivity of Cu_2O . We previously reported the crystal plane-dependent reducibility of Cu_2O cubes and octahedra in both H_2 and CO atmospheres²⁸ and the crystal plane-dependent oxidative dissolution of Cu_2O cubes, octahedra, and rhombic dodecahedra in a weak acid solution.²⁹ The coordination-oxidative dissolution of Cu_2O in aqueous ammonia solution is also a typical chemical

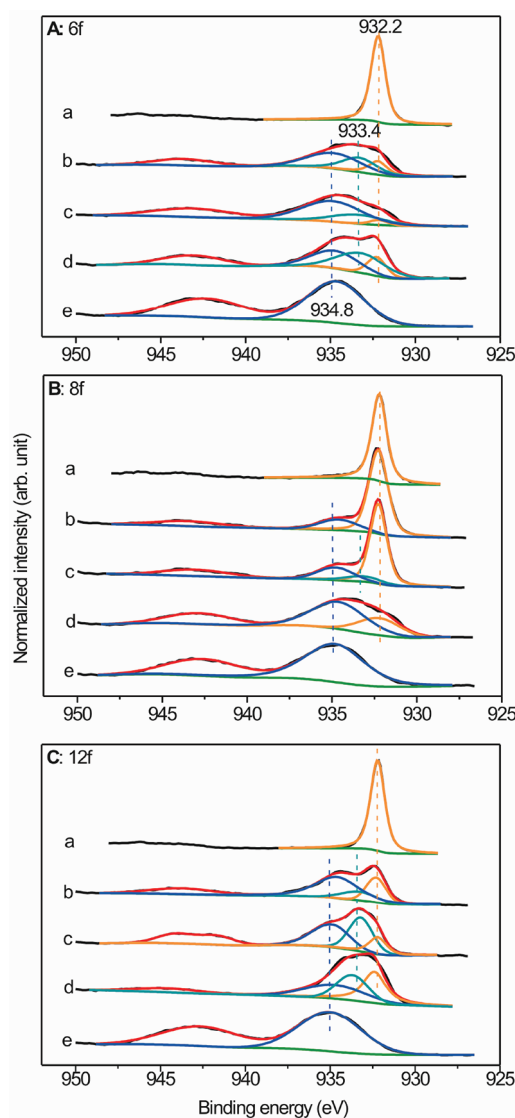


Figure 2. Cu 2p_{3/2} XPS spectra of (A) cubic (6f), (B) octahedral (8f), and (C) rhombic dodecahedral (12f) Cu_2O nanocrystals: (a) as-synthesized Cu_2O nanocrystals; Cu_2O nanocrystals etched in aqueous ammonia solution with $\text{pH} = 10.5$ for (b) 10 min and (c) 150 min; Cu_2O nanocrystals etched in aqueous ammonia solution with $\text{pH} = 11.4$ for (d) 3 min and (e) 40 min.

reaction occurring at the oxide-solution interface. In this manuscript, we have comprehensively investigated the compositional and morphological evolution of Cu_2O cubes, octahedra, and rhombic dodecahedra in aqueous ammonia solutions. The crystal plane-dependent structural evolution of Cu_2O nanocrystals was unambiguously identified in which the stability of different Cu_2O crystal planes in the aqueous ammonia solutions follows the order of $\{100\} > \{111\} > \{110\}$. It was also observed that the nucleation and growth behavior of reaction products ($\text{Cu}(\text{OH})_2$ and CuO precipitates) depends on the crystal plane exposed on Cu_2O nanocrystals.

2. EXPERIMENTAL SECTION

2.1. Synthesis of Cu_2O Nanocrystals. Five types of Cu_2O nanocrystals were prepared. All the chemicals were analytical grade reagents and were used as received without further

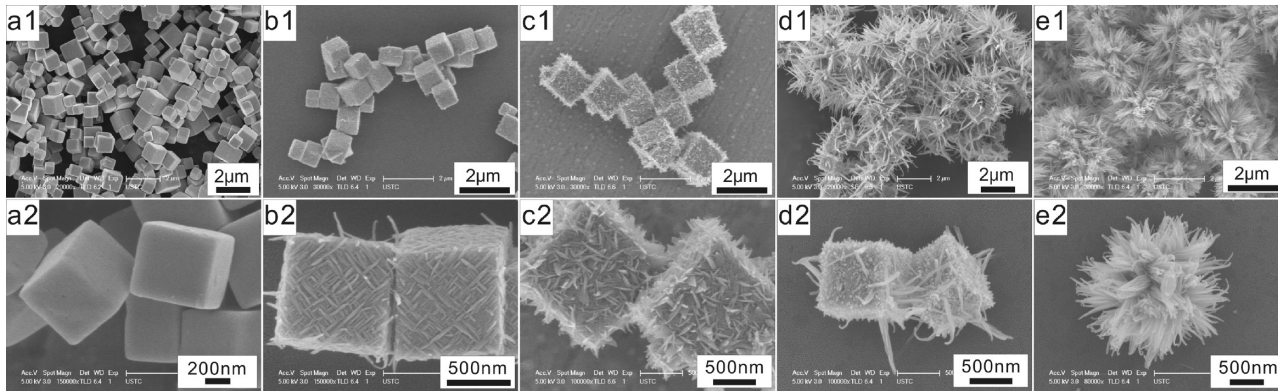


Figure 3. SEM images of as-synthesized Cu_2O cubes (a1 and a2), as-synthesized Cu_2O nanocubes etched in aqueous ammonia solution with $\text{pH} = 10.5$ for 10 min (b1 and b2) and 150 min (c1 and c2), and in aqueous ammonia solution with $\text{pH} = 11.4$ for 3 min (d1 and d2) and 40 min (e1 and e2).

purification. The synthesis of cubic, octahedral, and {100} truncated octahedral Cu_2O nanocrystals followed Zhang et al.'s recipe.⁸ In a typical procedure, 5.0 mL NaOH aqueous solution (2.0 mol/L) was added dropwise into 50 mL CuCl_2 aqueous solution (0.01 mol/L) containing different amounts of polyvinylpyrrolidone (PVP, MW = 30 000) (cube: 0 g; octahedra: 4.44 g; {100} truncated octahedra: 1.67 g) at 55 °C. After adequately stirring for 0.5 h, 5.0 mL ascorbic acid aqueous solution (0.6 mol/L) was added dropwise into the solution. The mixed solution was adequately stirred for different times (cubic: 5 h; octahedral: 3 h; {100} truncated octahedral: 3 h) at 55 °C. The resulting precipitate was collected by centrifugation and decanting and then was washed with distilled water and absolute ethanol and was finally dried in vacuum at room temperature (RT) for 12 h.

The synthesis of rhombic dodecahedral and {110} truncated octahedral Cu_2O nanocrystals followed Liang et al.'s recipe.⁹ In a typical procedure, 1 mmol CuSO_4 was dissolved in 40 mL water to form a clear solution into which different amounts of oleic acid (rhombic dodecahedra: 4 mL; {110} truncated octahedra: 3.5 mL) and 20 mL absolute ethanol were added successively with vigorous stirring. When the mixture was heated to 100 °C, 10 mL NaOH solution (8 mmol) was added. After 5 min, 30 mL aqueous solution containing 3.42 g D-(+)-glucose was added under constant stirring. The mixture reacted for another 60 min, and a brick-red color gradually appeared. The resulting precipitate was collected by centrifugation and decantation and then was washed with distilled water and absolute ethanol and finally was dried in vacuum at RT for 12 h.

2.2. Etching of Cu_2O Nanocrystals in Aqueous Ammonia Solution. Twenty milligrams of Cu_2O nanocrystals was dispersed into 40 mL aqueous ammonia solution ($\text{pH} = 10.5$ or 11.4). The mixture was stirred with a magnetic stirrer at 500 rpm. At desirable reaction times, the precipitate in the aqueous solution was collected by centrifugation, then was washed with distilled water and absolute ethanol, and finally was stored in absolute ethanol.

2.3. Structural Characterization. Powder X-ray diffraction (XRD) patterns were recorded on a Philips X'Pert PRO diffractometer using a nickel-filtered $\text{Cu K}\alpha$ (wavelength: 0.15418 nm) radiation source with the operation voltage and operation current being 40 kV and 40 mA, respectively. X-ray photoelectron spectroscopy (XPS) measurements were performed on an ESCALAB 250 high-performance electron spectrometer using monochromatized $\text{Al K}\alpha$ ($h\nu = 1486.7$ eV) as the

excitation source. The likely charging of samples was corrected by setting the binding energy of the adventitious carbon (C 1s) to 284.8 eV. Scanning electron microscope (SEM) experiments were performed on an FEI Sirion200 field emission scanning electron microscope operated at beam energy of 5.0 kV. Transmission electron microscopy (TEM) and selected area electron diffraction (SAED) experiments were preformed on JEOL-2010 and JEOL-2100F high-resolution transmission electron microscopes with electron acceleration energy of 200 kV.

3. RESULTS AND DISCUSSION

Curves a in Figure 1A–C show XRD patterns of as-synthesized cubic, octahedral, and rhombic dodecahedral Cu_2O nanocrystals confirming their crystal phases to be cubic fcc Cu_2O structure (JCPDS card no. 78-2076). The (200) diffraction peak in the XRD pattern of cubic Cu_2O nanocrystals is stronger than other diffraction peaks agreeing that cubic Cu_2O nanocrystals exclusively expose {100} crystal planes. Similar results also hold for the (111) diffraction peak in the XRD pattern of octahedral Cu_2O nanocrystals exclusively exposing {111} crystal planes and for the (220) diffraction peak in the XRD pattern of rhombic dodecahedral Cu_2O nanocrystals exclusively exposing {110} crystal planes. Curves a in Figure 2A–C show $\text{Cu 2p}_{3/2}$ XPS spectra of as-synthesized cubic, octahedral, and rhombic dodecahedral Cu_2O nanocrystals in which only a single component with a $\text{Cu 2p}_{3/2}$ binding energy at 932.2 eV corresponding to Cu(I) in Cu_2O appears. These results demonstrate that the surface composition of as-synthesized cubic, octahedral, and rhombic dodecahedral Cu_2O nanocrystals remains as Cu_2O . SEM images of cubic (a1 and a2 in Figure 3), octahedral (a1 and a2 in Figure 5), and rhombic dodecahedral (a1 and a2 in Figure 7) Cu_2O nanocrystals demonstrate that three types of Cu_2O nanocrystals have very uniform morphology. Cubic Cu_2O nanocrystals have a size of 400–700 nm, octahedral Cu_2O nanocrystals have a size of about 500 nm, and rhombic dodecahedral Cu_2O nanocrystals have a size of 600–900 nm.

3.1. Etching of Cubic Cu_2O Nanocrystals in Aqueous Ammonia Solution. Curves b and c in Figure 1A show XRD patterns of the precipitate after as-synthesized cubic Cu_2O nanocrystals were etched in aqueous ammonia solution with $\text{pH} = 10.5$ for 10 and 150 min, respectively. All observed diffraction peaks could be indexed to cubic fcc Cu_2O . However, in the corresponding $\text{Cu 2p}_{3/2}$ XPS spectra (curves b and c in Figure 2A), the Cu_2O component becomes weak and two new

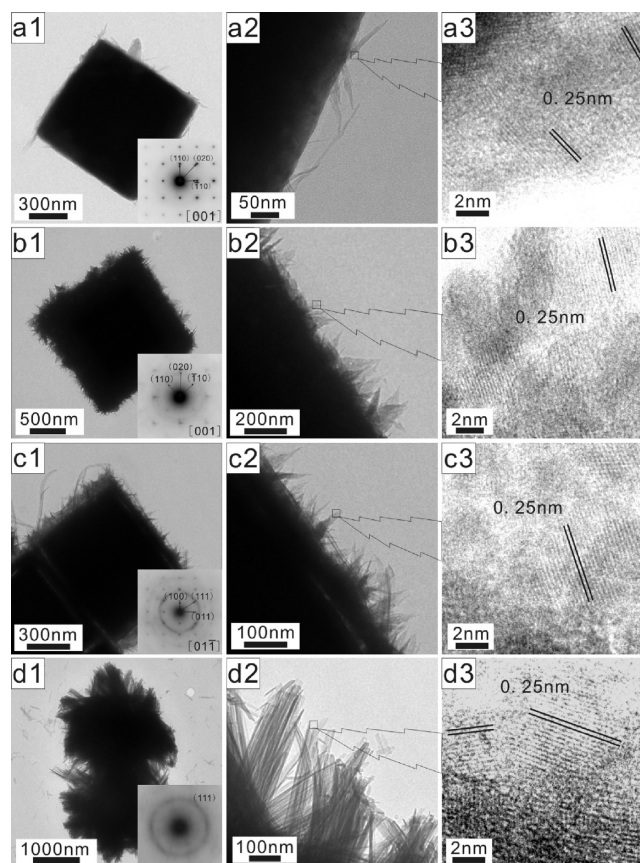


Figure 4. TEM images of as-synthesized cubic Cu_2O nanocrystals etched in aqueous ammonia solution with different pH values for different times: (a1)–(a3): 10 min with pH = 10.5; (b1)–(b3): 150 min with pH = 10.5; (c1)–(c3): 3 min with pH = 11.4; (d1)–(d3): 40 min with pH = 11.4. The insets in a1, b1, c1, and d1 show the corresponding SAED patterns.

components appear with $\text{Cu} 2\text{p}_{3/2}$ binding energies at 934.8 and 933.4 eV that could be assigned to $\text{Cu}(\text{OH})_2$ and CuO . The XPS results also indicate that, with the etching reaction proceeding, the $\text{Cu}(\text{OH})_2$ component grows at the expense of CuO and Cu_2O components. Thus, these experimental results suggest that CuO and $\text{Cu}(\text{OH})_2$ are formed during the etching reaction of cubic Cu_2O nanocrystals in aqueous ammonia solution, but their structures are beyond the detection limit of XRD.

When the pH value of aqueous ammonia solution increases to 11.4, the XRD pattern of the precipitate (Figure 1A d) still remains as that of cubic fcc Cu_2O after 3 min of etching reaction, and the corresponding $\text{Cu} 2\text{p}_{3/2}$ XPS spectrum (Figure 2A d) shows the coexistence of $\text{Cu}(\text{OH})_2$, CuO , and Cu_2O components; however, after 40 min of etching reaction, the XRD pattern of the precipitate (Figure 1A e) mainly displays the diffraction peaks of $\text{Cu}(\text{OH})_2$ (JCPDS card no. 72-0140) although the Cu_2O (111) and (200) diffraction peaks are still visible; meanwhile, the corresponding $\text{Cu} 2\text{p}_{3/2}$ XPS spectrum (Figure 2A e) only shows the existence of $\text{Cu}(\text{OH})_2$ component and not Cu_2O or CuO components.

The morphology of the precipitates after the etching of as-synthesized cubic Cu_2O nanocrystals in aqueous ammonia solution was studied by SEM and TEM. After the etching reaction proceeds in aqueous ammonia solution with pH = 10.5 for 10 min, SEM images (b1 and b2 in Figure 3) clearly evidence the

appearance of needlelike nanostructures on the surfaces of cubic Cu_2O nanocrystals. These needlelike nanostructures mostly lie on the surfaces of cubic Cu_2O nanocrystals. The accompanying TEM images (a1 and a2 in Figure 4) also demonstrate the formation of a dense overlayer on the surfaces of cubic Cu_2O nanocrystals after the etching reaction. The SAED pattern of the surface region (inset in Figure 4 a1) only gives that of Cu_2O (001) single crystal, which together with previous XRD results proves the poor crystallinity of formed needlelike nanostructures. The poorly crystallized needlelike nanostructure is quite common for hydroxide. Thus, the needlelike nanostructures formed on the surfaces of cubic Cu_2O nanocrystals during the etching in aqueous ammonia solution can be assigned to $\text{Cu}(\text{OH})_2$. The HRTEM image (Figure 4 a3) reveals a lattice fringe of 0.25 nm of the overlayer that corresponds to the lattice fringe of $\text{Cu}(\text{OH})_2$ (111) crystal plane. However, the lattice fringe of CuO ($\bar{1}11$) crystal plane is also 0.25 nm, and XPS results also demonstrate the existence of CuO ; therefore, it is likely that ultrafine CuO particles coexist with $\text{Cu}(\text{OH})_2$ nanostructures. With the etching time prolonging to 150 min, both SEM (c1 and c2 in Figure 3) and TEM (b1–b3 in Figure 4) images demonstrate that the formed $\text{Cu}(\text{OH})_2$ needlelike nanostructures become much denser and thicker and extend outside from the surfaces of cubic Cu_2O nanocrystals.

When the pH of the aqueous ammonia solution increases to 11.4, the etching reaction proceeds quickly, and the dense and thick needlelike $\text{Cu}(\text{OH})_2$ nanostructure forms on the surfaces of cubic Cu_2O nanocrystals and extends outside (d1 and d2 in Figure 3 and c1–c3 in Figure 4). The SAED pattern of the surface region (inset in Figure 4 c1) gives both the ED pattern of Cu_2O (100) single crystal and the incomplete ED pattern of polycrystalline $\text{Cu}(\text{OH})_2$ (111) crystal plane. With the etching reaction proceeding for 40 min, SEM images (e1 and e2 in Figure 3) show that needlelike $\text{Cu}(\text{OH})_2$ nanostructures become dense nanobelts longer than 500 nm and cubic Cu_2O nanocrystals could be hardly observed. A single particle looks like an urchin. The corresponding TEM images (d1–d3 in Figure 4) confirm the presence of fine cubic Cu_2O nanocrystals enclosed by dense and long $\text{Cu}(\text{OH})_2$ nanobelts. The SAED patterns of the surface region (inset in Figure 4 d1) only give the ED ring pattern of polycrystalline $\text{Cu}(\text{OH})_2$ (111) crystal plane. From their morphology, it can be thus deduced that the absence of Cu_2O and CuO component in the $\text{Cu} 2\text{p}_{3/2}$ XPS spectrum after 40 min of etching of cubic Cu_2O nanocrystals in the aqueous ammonia solution with pH = 11.4 is due to the existence of the dense and thick $\text{Cu}(\text{OH})_2$ overlayer since XPS is a surface-sensitive technique.

Therefore, on the basis of the above experimental observations, the compositional and structural evolution of cubic Cu_2O nanocrystals in aqueous ammonia solution could be deduced as the following: poorly crystallized needlelike $\text{Cu}(\text{OH})_2$ nanostructures and ultrafine CuO particles initially nucleate and grow on the surfaces of cubic Cu_2O nanocrystals, and then cubic Cu_2O nanocrystal (core)/needlelike $\text{Cu}(\text{OH})_2$ and ultrafine CuO particle (shell) nanocomposites develop; with the etching reaction proceeding or with the pH value of aqueous ammonia solution increasing, the cubic Cu_2O nanocrystal core keeps shrinking whereas the needlelike $\text{Cu}(\text{OH})_2$ nanostructures in the shell grow dense and thick and eventually develop into long $\text{Cu}(\text{OH})_2$ nanobelts. However, cubic Cu_2O nanocrystals can survive in aqueous ammonia solution under our experimental conditions.

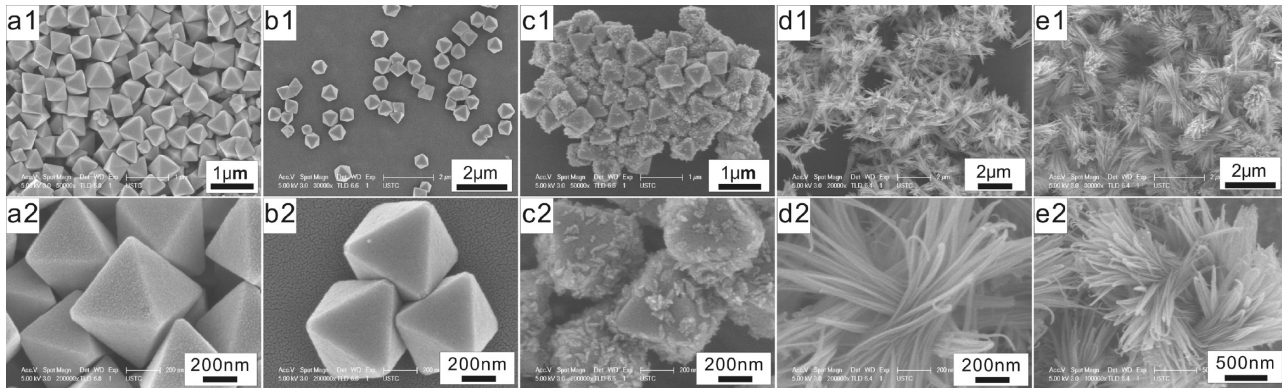


Figure 5. SEM images of as-synthesized Cu_2O octahedra (a1 and a2), as-synthesized Cu_2O nanoctahedra etched in aqueous ammonia solution with $\text{pH} = 10.5$ for 10 min (b1 and b2) and 150 min (c1 and c2), and in aqueous ammonia solution with $\text{pH} = 11.4$ for 3 min (d1 and d2) and 40 min (e1 and e2).

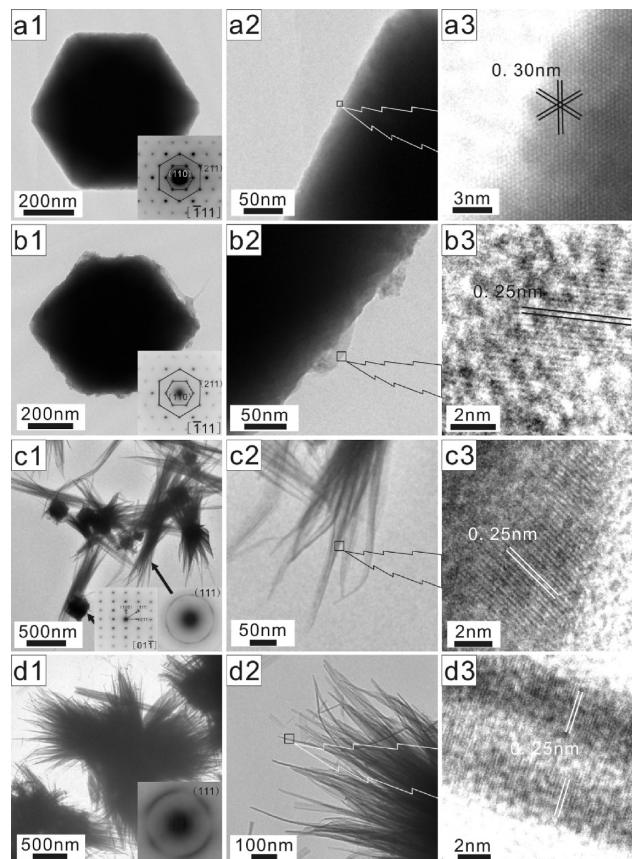


Figure 6. TEM images of as-synthesized octahedral Cu_2O nanocrystals etched in aqueous ammonia solution with different pH values for different times: (a1–a3) 10 min with $\text{pH} = 10.5$; (b1–b3) 150 min with $\text{pH} = 10.5$; (c1–c3) 3 min with $\text{pH} = 11.4$; (d1–d3) 40 min with $\text{pH} = 11.4$. The insets in a1, b1, c1, and d1 show the corresponding SAED patterns.

3.2. Etching of Octahedral Cu_2O Nanocrystals in Aqueous Ammonia Solution. Curves b and c in Figure 1B show XRD patterns of the precipitate after as-synthesized octahedral Cu_2O nanocrystals were etched in aqueous ammonia solution with $\text{pH} = 10.5$ for 10 and 150 min, respectively. Similar to the case of cubic Cu_2O nanocrystals, only diffraction peaks from cubic fcc

Cu_2O were observed. In the corresponding $\text{Cu} 2\text{p}_{3/2}$ XPS spectra (curves b and c in Figure 2B), the Cu_2O component is almost as strong as that of as-synthesized octahedral Cu_2O nanocrystals, and only the $\text{Cu}(\text{OH})_2$ component appears after 10 min of etching reaction, and both $\text{Cu}(\text{OH})_2$ and CuO components appear after 150 min of etching reaction. These results are in contrast to the case of cubic Cu_2O nanocrystals. When the pH value of aqueous ammonia solution increases to 11.4, the XRD pattern of the precipitate (Figure 1B d) still remains as that of cubic fcc Cu_2O after 3 min of etching reaction, and the corresponding $\text{Cu} 2\text{p}_{3/2}$ XPS spectrum (Figure 2B d) shows $\text{Cu}(\text{OH})_2$ and Cu_2O components. Comparing those after etching in aqueous ammonia solution with $\text{pH} = 10.5$, the intensity of Cu_2O component is substantially reduced. After 40 min of etching reaction, the XRD pattern of the precipitate (Figure 1B e) only displays the diffraction peaks of $\text{Cu}(\text{OH})_2$ and the corresponding $\text{Cu} 2\text{p}_{3/2}$ XPS spectrum (Figure 2B e) only shows the $\text{Cu}(\text{OH})_2$ component.

Surprisingly, SEM images of the precipitates after the etching of as-synthesized octahedral Cu_2O nanocrystals in aqueous ammonia solution with $\text{pH} = 10.5$ for 10 min (b1 and b2 in Figure 5) seem to be the same as those of as-synthesized octahedral Cu_2O nanocrystals, and the corresponding TEM images (a1–a3 in Figure 6) also do not show any novel structures on the surfaces of octahedral Cu_2O nanocrystals. These microscopic results well explain the XPS observation that the Cu_2O component of the precipitate after 10 min of etching in aqueous ammonia solution with $\text{pH} = 10.5$ is almost as strong as that of as-synthesized octahedral Cu_2O nanocrystals. However, the XPS results also demonstrate the formation of $\text{Cu}(\text{OH})_2$; therefore, we proposed that $\text{Cu}(\text{OH})_2$ might nucleate and grow in the aqueous solution instead of on the surfaces of octahedral Cu_2O nanocrystals when as-synthesized octahedral Cu_2O nanocrystals were etched in aqueous ammonia solution. With the etching time prolonging to 150 min, SEM images (c1 and c2 in Figure 5) clearly show that irregular nanostructures loosely disperse on the surfaces of octahedral Cu_2O nanocrystals. This is also confirmed by TEM images (b1 and b2 in Figure 6). The HRTEM image (Figure 6 b3) reveals the lattice fringe of 0.25 nm of the nanostructures that could arise from the lattice fringes of $\text{Cu}(\text{OH})_2$ (111) crystal plane or of CuO ($\bar{1}\bar{1}1$) crystal plane.

The etching reaction of as-synthesized octahedral Cu_2O nanocrystals proceeds quickly in aqueous ammonia solution

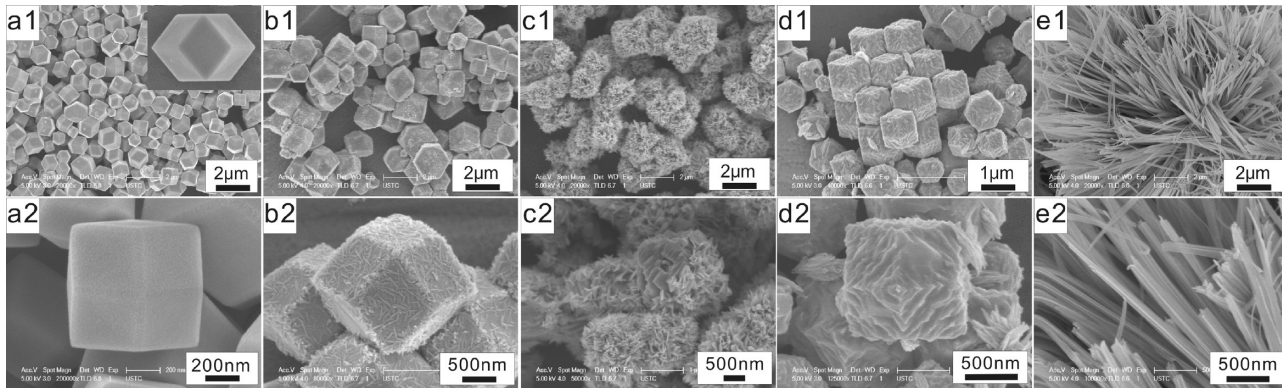


Figure 7. SEM images of as-synthesized Cu₂O rhombic dodecahedra (a1 and a2), as-synthesized Cu₂O rhombic dodecahedra etched in aqueous ammonia solution with pH = 10.5 for 10 min (b1 and b2) and 150 min (c1 and c2), and in aqueous ammonia solution with pH = 11.4 for 3 min (d1 and d2) and 40 min (e1 and e2).

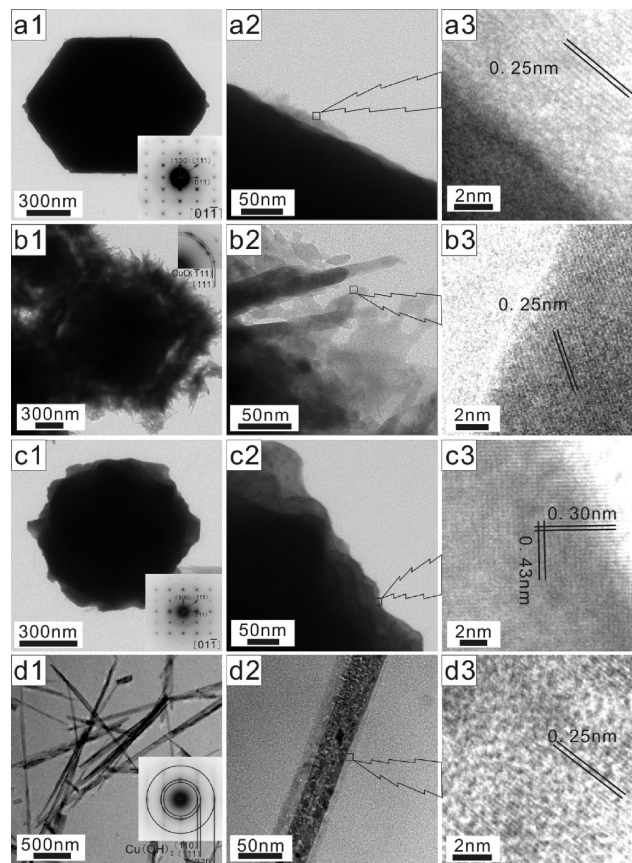


Figure 8. TEM images of as-synthesized rhombic dodecahedral Cu₂O nanocrystals etched in aqueous ammonia solution with different pH values for different times: (a1–a3) 10 min with pH = 10.5; (b1–b3) 150 min with pH = 10.5; (c1–c3) 3 min with pH = 11.4; (d1–d3) 40 min with pH = 11.4. The insets in a1, b1, c1, and d1 show the corresponding SAED patterns.

with pH = 11.4. After 3 min of etching, only bunches of Cu(OH)₂ nanobelts can be seen in the SEM images (d1 and d2 in Figure 5), although the existence of Cu₂O nanocrystals is evident in XRD and XPS results. However, the corresponding TEM image (Figure 6 c1) observes small cubelike nanocrystals and long nanobelts whose compositions are verified by the

accompanying SAED patterns (insets in Figure 6 c1) to be Cu₂O and Cu(OH)₂, respectively. It can be seen clearly that Cu(OH)₂ nanobelts locate beside Cu₂O nanocrystals supporting our argument that Cu(OH)₂ might nucleate and grow in the aqueous solution instead of on the surfaces of octahedral Cu₂O nanocrystals when as-synthesized octahedral Cu₂O nanocrystals are etched in aqueous ammonia solution. This observation greatly differs from the case for cubic Cu₂O nanocrystals in which cubic Cu₂O nanocrystal (core)/Cu(OH)₂ nanobelt (shell) nanocomposites form. As-synthesized octahedral Cu₂O nanocrystals were completely etched away after etched in aqueous ammonia solution with pH = 11.4 for 40 min, and SEM (e1 and e2 in Figure 5) and TEM images (d1–d3 in Figure 6) only observe Cu(OH)₂ nanobelts.

Therefore, on the basis of the above experimental observations, the compositional and structural evolution of octahedral Cu₂O nanocrystals in aqueous ammonia solution could be deduced as the following: major Cu(OH)₂ nanostructures nucleate and grow in the aqueous ammonia solution and minor Cu(OH)₂ and CuO nanostructures sparsely nucleate and grow on the surfaces of octahedral Cu₂O nanocrystals. Octahedral Cu₂O nanocrystals can be etched away in aqueous ammonia solution with pH = 11.4 forming Cu(OH)₂ nanobelts.

3.3. Etching of Rhombic Dodecahedral Cu₂O Nanocrystals in Aqueous Ammonia Solution. The precipitate after etching of as-synthesized rhombic dodecahedral Cu₂O nanocrystals in aqueous ammonia solution with pH = 10.5 for 10 min only exhibits diffraction peaks from cubic fcc Cu₂O in its XRD pattern (Figure 1C b) and Cu₂O component with a reduced intensity and new Cu(OH)₂ and CuO components in its (Figure 2C b). However, after the etching reaction proceeding for 150 min, the precipitate exhibits diffraction peaks not only from cubic fcc Cu₂O but also from CuO (JCPDS card no. 89-5899) in its XRD pattern (Figure 1C c) demonstrating the formation of large CuO crystallites which is not observed in the cases of cubic and octahedral Cu₂O nanocrystals. In the corresponding Cu 2p_{3/2} XPS spectrum (Figure 2C c), both Cu(OH)₂ and CuO components grow at the expense of Cu₂O component. When the pH value of aqueous ammonia solution increases to 11.4, the XRD pattern of the precipitate (Figure 1C d) remains as that of cubic fcc Cu₂O after 3 min of etching reaction, and the corresponding Cu2p_{3/2} XPS spectrum (Figure 2C d) shows Cu₂O, Cu(OH)₂, and CuO components. After 40 min of etching reaction, the

precipitate only displays the diffraction peaks of $\text{Cu}(\text{OH})_2$ in the XRD pattern (Figure 1C e) that are sharper than those of $\text{Cu}(\text{OH})_2$ formed by the etching of cubic and octahedral Cu_2O nanocrystals under the same condition suggesting their better crystallinity. The corresponding Cu 2p_{3/2} XPS spectrum (Figure 2C e) only shows the $\text{Cu}(\text{OH})_2$ component.

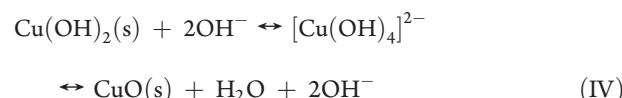
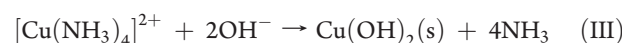
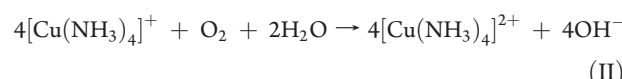
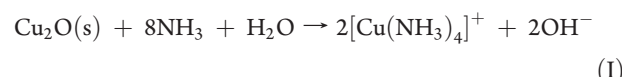
On the surfaces of rhombic dodecahedral Cu_2O nanocrystals etched in aqueous ammonia solution with pH = 10.5 for 10 min, small particles and needlelike nanostructures coexist (b1 and b2 in Figure 7) that might, respectively, correspond to CuO and $\text{Cu}(\text{OH})_2$. The corresponding TEM images (a1–a3 in Figure 8) also confirm these results. With the etching time prolonging to 150 min, a quite uniform nanostructure forms (Figure 7 c1). Indicated by the SEM image of a broken nanostructure (Figure 7 c2), the Cu_2O (core)/ $\text{Cu}(\text{OH})_2$ and CuO (shell) structure can be observed. Interestingly, the Cu_2O core does not keep the original rhombic dodecahedral shape but exhibits stepped square facets with different sizes. The Cu_2O (core)/ $\text{Cu}(\text{OH})_2$ and CuO (shell) structure is further confirmed by the corresponding TEM image (Figure 8 b1). The SAED pattern of the shell region (inset in Figure 8 b1) shows the CuO diffraction pattern agreeing with the XRD results. Rodlike nanostructures with a lattice fringe of 0.25 nm (b2 and b3 in Figure 8) exist in the shell region and can be assigned to CuO crystallites.

When etched in the pH = 11.4 aqueous ammonia solution for 3 min, rhombic dodecahedral Cu_2O nanocrystals rough preserve their shape but with newly formed stepped square facets with different sizes (d1 and d2 in Figure 7); meanwhile, some nanobelts can be found nearby. In this case, the lattice fringe of stepped square facets can be seen clearly resolved by HRTEM (Figure 8 c3) that demonstrates that the square facets expose the $\text{Cu}_2\text{O}(100)$ crystal plane. After etched for 40 min, both SEM (e1 and e2 in Figure 7) and TEM (d1–d3 in Figure 8) images only demonstrate the existence of $\text{Cu}(\text{OH})_2$ nanobelts.

Therefore, on the basis of the above experimental results, the compositional and structural evolution of rhombic dodecahedral Cu_2O nanocrystals in aqueous ammonia solution could be deduced as the following: $\text{Cu}(\text{OH})_2$ and CuO nanostructures not only nucleate and grow on the surfaces of Cu_2O nanocrystals, forming Cu_2O (core)/ $\text{Cu}(\text{OH})_2$ and CuO (shell) structure in which CuO grows into large crystallites, but also nucleate and grow the aqueous ammonia solution. Interestingly, Cu_2O square facets exposing {100} crystal planes were observed to form at the expense of original {110} crystal planes during the etching reaction. Octahedral Cu_2O nanocrystals can be etched away in aqueous ammonia solution with pH = 11.4 forming $\text{Cu}(\text{OH})_2$ nanobelts.

3.4. Reaction Mechanism of the Etching of Cu_2O Nanocrystals in Aqueous Ammonia Solution. The above experimental results demonstrate that Cu_2O nanocrystals can be etched in aqueous ammonia solution. Park et al.²⁴ reported that aqueous ammonia solution could convert Cu_2O nanocubes to polycrystalline CuO hollow nanostructures in air through a sequential dissolution–precipitation process and that increasing the pH value of the solution led to the formation of hollow cubes, hollow spheres, and urchinlike particles. In our experiments, both $\text{Cu}(\text{OH})_2$ and CuO precipitates were observed as the solid products after Cu_2O was etched in aqueous ammonia solution with pH = 10.5 within 150 min or in aqueous ammonia solution with pH = 11.4 for 3 min, but the $\text{Cu}(\text{OH})_2$ precipitate with a nanobelt morphology is the only solid product after Cu_2O was etched in aqueous ammonia solution with pH = 11.4 for 40 min.

Such etching processes of Cu_2O nanocrystals were not observed in aqueous NaOH solutions with the same pH values as aqueous ammonia solutions. Therefore, the etching processes should be initiated by the coordination of Cu_2O with NH_3 to form $[\text{Cu}(\text{NH}_3)_4]^{+}$.²⁴ $[\text{Cu}(\text{NH}_3)_4]^{+}$ can be oxidized by dissolved O_2 to produce $[\text{Cu}(\text{NH}_3)_4]^{2+}$ that then slowly precipitates in aqueous ammonia solution to produce $\text{Cu}(\text{OH})_2$. The transformation mechanism between $\text{Cu}(\text{OH})_2$ and CuO is not clear, but $[\text{Cu}(\text{OH})_4]^{2-}$ was previously proposed as the intermediate.²¹ Our results suggest that aqueous ammonia solution with a high pH value should favor the formation of $\text{Cu}(\text{OH})_2$ precipitate. Therefore, the etching of Cu_2O nanocrystals in aqueous ammonia solution can be described by the following sequential coordination dissolution–oxidation–precipitation reaction mechanism:



It can be seen that the etching of Cu_2O nanocrystals in aqueous ammonia solution involves two types of solid–liquid interfacial reactions. One is the coordinative dissolution of Cu_2O nanocrystals, and the other is the precipitation of $\text{Cu}(\text{OH})_2$ and CuO .

3.5. Crystal Plane-Dependent Nucleation and Growth of $\text{Cu}(\text{OH})_2$ and CuO Precipitates. It is always the solid surface that participates in the solid–liquid interfacial reaction, and thus, the surface structure of a solid could exert influences on the solid–liquid interfacial reaction. Our experimental results clearly demonstrate that the shape of Cu_2O nanocrystals, that is, the crystal plane exposed on Cu_2O nanocrystals, strongly influences the etching processes. An obvious experimental observation is that the nucleation and growth of $\text{Cu}(\text{OH})_2$ precipitate depend on the crystal plane exposed on Cu_2O nanocrystals. For cubic Cu_2O nanocrystals, $\text{Cu}(\text{OH})_2$ nanostructures mainly nucleate and grow on the surface of cubic Cu_2O nanocrystals forming cubic Cu_2O nanocrystal (core)/ $\text{Cu}(\text{OH})_2$ nanobelt (shell) nanostructures. For octahedral Cu_2O nanocrystals, most $\text{Cu}(\text{OH})_2$ nanostructures nucleate and grow into $\text{Cu}(\text{OH})_2$ nanobelts in the aqueous ammonia solution, and only minor $\text{Cu}(\text{OH})_2$ nanostructures sparsely nucleate and grow on the surfaces of octahedral Cu_2O nanocrystals. For rhombic dodecahedral Cu_2O nanocrystals, $\text{Cu}(\text{OH})_2$ nanostructures nucleate and grow both on the surfaces of Cu_2O nanocrystals and in the aqueous ammonia solution. Our results also indicate that CuO mainly nucleates and grows on the surface of Cu_2O nanocrystals for all cubic, octahedral, and rhombic dodecahedral Cu_2O nanocrystals in which ultrafine CuO particles beyond the detection of XRD are formed for cubic and octahedral Cu_2O nanocrystals, but large

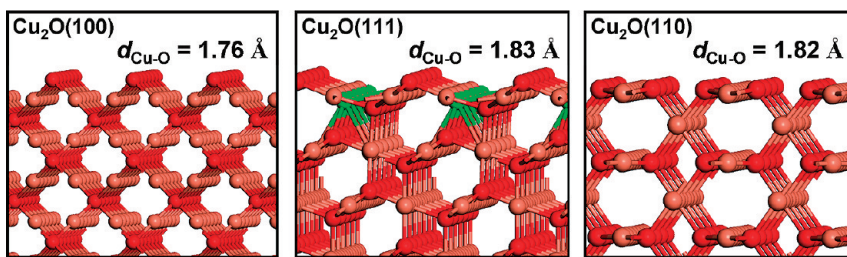


Figure 9. Optimized structures of Cu_2O (100), (111), and (110) surfaces. The red, brick, and green balls represent oxygen, coordinated saturated copper (Cu_{CSA}), and coordinated unsaturated copper (Cu_{CUS}) atoms, respectively. The distance between the nearest-neighboring $\text{Cu}(\text{I})$ and O on different surfaces is also indicated.

CuO crystallites detected by XRD are formed for rhombic dodecahedral Cu_2O nanocrystals.

Figure 9 shows the optimized surface structure of Cu_2O (100), (111), and (110) surfaces selectively exposed on cubic, octahedral, and rhombic dodecahedral Cu_2O nanocrystals, respectively.^{28,29} It can be clearly seen that different Cu_2O surfaces consist of Cu and O with different coordination environments and different surface Cu:O stoichiometries. The etching of Cu_2O nanocrystals in aqueous ammonia solution initiates from the coordination of $\text{Cu}(\text{I})$ in Cu_2O with NH_3 to produce $[\text{Cu}(\text{NH}_3)_4]^+$, and oxygen anions bonded with $\text{Cu}(\text{I})$ in Cu_2O subsequently react with H_2O to produce OH^- . Therefore, the coordination environment of $\text{Cu}(\text{I})$ in Cu_2O surface that is closely related with its reactivity and the surface Cu:O stoichiometric on Cu_2O nanocrystals that might affect local concentrations of $[\text{Cu}(\text{NH}_3)_4]^+$ and OH^- at the liquid–solid interface should play important roles in the observed different etching behaviors of cubic, octahedral, and rhombic dodecahedral Cu_2O nanocrystals in aqueous ammonia solution.

On $\text{Cu}_2\text{O}(100)$ surface, the first layer consists of coordinated unsaturated O (O_{CUS}) and the second layer consists of coordinated saturated Cu (Cu_{CSA}). The etching reaction initiates from the coordination reaction of Cu_{CSA} in the second layer, and O_{CUS} in the first layer simultaneously gets released and reacts with H_2O to produce OH^- . In bulk Cu_2O , Cu is coordinated to two O, and O is coordinated to four Cu to give a Cu:O stoichiometric of 2; however, on the $\text{Cu}_2\text{O}(100)$ surface, O in the first layer is only coordinated to two Cu, and Cu in the second layer is also coordinated to two O; therefore, we consider that the surface Cu:O stoichiometric on $\text{Cu}_2\text{O}(100)$ is 1. Thus, the $[\text{OH}^-]$ is high at the liquid– Cu_2O interface, which facilitates formation of $\text{Cu}(\text{OH})_2$ precipitate at the liquid– Cu_2O interface. This results in the observed nucleation and growth of $\text{Cu}(\text{OH})_2$ precipitate on the surface of cubic Cu_2O nanocrystals.

On $\text{Cu}_2\text{O}(111)$ surface, the first layer consists of (O_{CUS}) and the second layer consists of Cu_{CSA} and coordinated unsaturated Cu (Cu_{CUS}). Cu_{CUS} in the second layer exhibits higher reactivity than Cu_{CSA} and undergoes the coordination reaction more facilely. The formation of $[\text{Cu}(\text{NH}_3)_4]^+$ from Cu_{CUS} only reduces the coordination number of coordination saturated O in the third layer of $\text{Cu}_2\text{O}(111)$ to which it is bonded and does not release any free O anions; thus, the local $[\text{OH}^-]$ concentration at the liquid–solid interface does not increase after the coordination of Cu_{CUS} in the second layer. Therefore, these $[\text{Cu}(\text{NH}_3)_4]^+$ can migrate away from the liquid–solid interface and undergo the subsequent oxidation and precipitation reaction in the aqueous ammonia solution. Meanwhile, $\text{Cu}_2\text{O}(111)$ surface is more open than $\text{Cu}_2\text{O}(100)$ surface; $[\text{Cu}(\text{NH}_3)_4]^+$

formed by the coordination reaction of Cu_{CSA} in the second layer also has more chances to migrate into the solution instead of occurring in reactions at the liquid– Cu_2O interface. This results in the observed nucleation and growth of most $\text{Cu}(\text{OH})_2$ nanostructures in the aqueous ammonia solution.

On $\text{Cu}_2\text{O}(110)$, the first layer consists of both O_{CUS} and Cu_{CSA} and the second layer consists of Cu_{CSA} . Cu_{CSA} in the first layer undergoes the coordination reaction more facilely. On one hand, this coordination reaction does not release any free O anions, and thus, the local $[\text{OH}^-]$ concentration at the liquid–solid interface does not increase, and thus, the formed $[\text{Cu}(\text{NH}_3)_4]^+$ can migrate away from the liquid–solid interface and can undergo the subsequent oxidation and precipitation reaction in the aqueous ammonia solution explaining the experimental observation that some $\text{Cu}(\text{OH})_2$ nanostructures nucleate and grow in the aqueous ammonia solution. On the other hand, this reaction further reduces the coordination number of coordination unsaturated O in the first layer of $\text{Cu}_2\text{O}(110)$ that is bonded with Cu_{CSA} in the first layer and thus results in its high reactivity. Therefore, after the coordination reaction of Cu_{CSA} in the first layer, the remaining surface structure of $\text{Cu}_2\text{O}(110)$ consists of the very low coordinated O_{CUS} in the first layer and Cu_{CSA} in the second layer, which we propose to be responsible for the formation of large CuO crystallites on the surface that were experimentally observed.

3.6. Crystal Plane-Dependent Stability of Cu_2O Nanocrystals in Aqueous Ammonia Solution. Under the most serious etching reaction condition employed in our experiments ($\text{pH} = 11.4$, $t = 40$ min), cubic Cu_2O nanocrystals can survive but octahedral and rhombic dodecahedral Cu_2O nanocrystals completely react off. This implies that cubic Cu_2O nanocrystals are more stable than octahedral and rhombic dodecahedral Cu_2O nanocrystals in the aqueous ammonia solution. We observed the formation of dense $\text{Cu}(\text{OH})_2$ and CuO layer on the surface of cubic Cu_2O nanocrystals which might act to suppress the coordination dissolution reaction of inner Cu_2O nanocrystals and thus might enhance their stability to a certain extent. However, we also observed the formation of $\{100\}$ facets at the expense of original $\{110\}$ crystal planes on the surface of rhombic dodecahedral Cu_2O nanocrystals etched in the aqueous ammonia solution indicating that $\text{Cu}_2\text{O}(100)$ surface is more stable. In other words, $\text{Cu}_2\text{O}(100)$ surface is less reactive than $\text{Cu}_2\text{O}(110)$ surface toward the coordination dissolution reaction.

To directly compare the stability of Cu_2O (111) and (110) surfaces in the aqueous ammonia solution, we synthesized $\{110\}$ truncated octahedral Cu_2O nanocrystals exposing both $\{110\}$ facets and $\{111\}$ planes whose SEM results are presented in

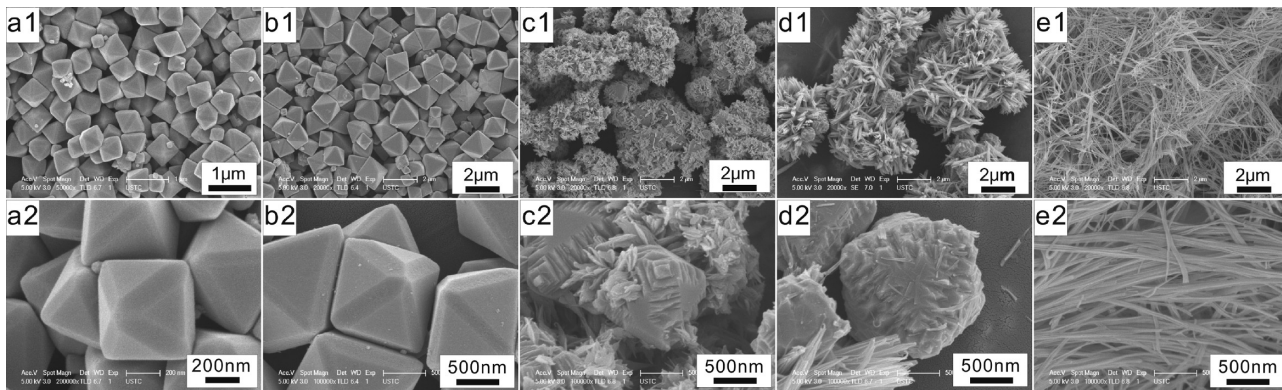


Figure 10. SEM images of (a1, a2) as-synthesized $\{110\}$ truncated Cu_2O octahedra. SEM images of as-synthesized $\{110\}$ truncated Cu_2O octahedra etched in aqueous ammonia solution with $\text{pH} = 10.5$ for (b1, b2) 10 min and (c1, c2) 150 min and in aqueous ammonia solution with $\text{pH} = 11.4$ for (d1, d2) 3 min and (e1, e2) 40 min.

Figure 10a. The size of $\{110\}$ truncated octahedral Cu_2O nanocrystals is between 500 and 700 nm. No obvious morphological change was observed by SEM after $\{110\}$ truncated octahedral Cu_2O nanocrystals were etched in the aqueous ammonia solution ($\text{pH} = 10.5$) for 10 min (Figure 10b). When the etching reaction was prolonged to 150 min, the square $\{100\}$ facets obviously formed on the $\{110\}$ faces of $\{110\}$ truncated octahedral Cu_2O nanocrystals and extended to the $\{111\}$ faces (Figure 10c), but the $\{111\}$ faces were still visible. After $\{110\}$ truncated octahedral Cu_2O nanocrystals were etched in the aqueous ammonia solution ($\text{pH} = 11.4$) for 3 min, similar results were observed. The square $\{100\}$ facets obviously formed on the $\{110\}$ facets of $\{110\}$ truncated octahedral Cu_2O nanocrystals and extended to the $\{111\}$ faces (Figure 10d), but the $\{111\}$ faces were still visible. Only $\text{Cu}(\text{OH})_2$ nanobelts were visible in the SEM images after being etched for 40 min (Figure 10e). Therefore, the experimental results of $\{110\}$ truncated octahedral Cu_2O nanocrystals demonstrate that $\text{Cu}_2\text{O}(111)$ surface is more stable than $\text{Cu}_2\text{O}(110)$ in the aqueous ammonia solution. In other words, $\text{Cu}_2\text{O}(111)$ surface is less reactive than $\text{Cu}_2\text{O}(110)$ surface toward the coordination dissolution reaction.

Therefore, we could establish that the stability of Cu_2O crystal planes in the aqueous ammonia solution follows the order $\{100\} > \{111\} > \{110\}$. This order is the same as that of the stability of Cu_2O crystal planes in the weak acid solution that we previously reported.²⁹ Cu_2O nanocrystals undergo the coordination dissolution reaction in the aqueous ammonia solution and the oxidative dissolution reaction in the weak acid solution. Both reactions occur at the liquid–solid interface and always initiate from the surface of Cu_2O nanocrystals, and both reactions involve the breaking of $\text{Cu}–\text{O}$ bond on the surface of Cu_2O nanocrystals. The strength of $\text{Cu}–\text{O}$ bond on the surface of Cu_2O nanocrystals should thus play a decisive role. Inferred from the optimized structures of Cu_2O (100), (111), and (110) surfaces (Figure 9), the distance between the nearest-neighboring O_{CUS} and Cu_{CSA} ($d(\text{Cu}_{\text{CSA}}–\text{O}_{\text{CUS}})$) on $\text{Cu}_2\text{O}(100)$ is 1.76 Å; the distance between the nearest-neighboring O_{CUS} and Cu_{CSA} on $\text{Cu}_2\text{O}(111)$ is 1.83 Å; the distance between the nearest-neighboring Cu_{CUS} and coordinated saturated O (O_{CSA}) ($d(\text{Cu}_{\text{CUS}}–\text{O}_{\text{CSA}})$) is 1.91 Å; the distance between the nearest-neighboring O_{CUS} and Cu_{CSA} ($d(\text{Cu}_{\text{CSA}}–\text{O}_{\text{CUS}})$) on $\text{Cu}_2\text{O}(110)$ is 1.82 Å. The $\text{Cu}–\text{O}$ bond on Cu_2O (100) is the shortest and thus the strongest; therefore, in view of the $\text{Cu}–\text{O}$

bond strength, the $\text{Cu}_2\text{O}(100)$ surface is the most stable for reactions involving the breaking of $\text{Cu}–\text{O}$ bond agreeing with our experimental results.

Therefore, various types of uniform Cu_2O nanocrystals can be successfully employed as model systems to fundamentally investigate the complex chemical reactions occurring at the liquid–solid interface. The crystal plane-dependent componential and morphological evolution of various types of uniform Cu_2O nanocrystals in the aqueous ammonia solution reported herein and in the weak acid solution that we previously reported²⁹ adequately demonstrates that the crystal plane exposed on solid crystals, that is, the surface structure of solid crystals, exerts a decisive role in their reactivity in reactions occurring at the liquid–solid interface. A solid particle usually exposes several different types of crystal planes on its surface that exhibit different reactivities under the same reaction condition. For chemical reactions involving the breaking of chemical bond, the crystal plane exposed on a solid particle whose chemical bond is the strongest is the most stable. The different reactivities of different types of crystal planes exposed on a solid particle determine its componential and morphological evolution under the reactive environment. These results might help us to understand the componential and morphological change of natural minerals with the change of the local chemical environment that the minerals experience.

4. CONCLUSIONS

We have comprehensively investigated the componential and morphological evolution of various types of uniform Cu_2O nanocrystals in aqueous ammonia solutions in which Cu_2O nanocrystals undergo a series of reactions to produce $\text{Cu}(\text{OH})_2$ and CuO precipitates. The shape of Cu_2O nanocrystals and thus of the crystal plane exposed on Cu_2O nanocrystals determines the surface structure and reactivity of Cu_2O nanocrystals. The stability of various types of uniform Cu_2O nanocrystals (various types of Cu_2O surfaces) in the aqueous ammonia solution follows the order cubic Cu_2O nanocrystals ($\text{Cu}_2\text{O}(100)$) > octahedral Cu_2O nanocrystals ($\text{Cu}_2\text{O}(111)$) > rhombic dodecahedral Cu_2O nanocrystals ($\text{Cu}_2\text{O}(110)$) agreeing with the order for the $\text{Cu}–\text{O}$ bond strength of Cu_2O (100), (111), and (110) surfaces. The nucleation and the growth of $\text{Cu}(\text{OH})_2$ and CuO precipitate that are closely related with its reactivity and the surface $\text{Cu}:\text{O}$ stoichiometric on Cu_2O nanocrystals also depend on the crystal plane

exposed on Cu₂O nanocrystals. These results well exemplify the crystal plane-dependent reactivity of oxide nanocrystals and greatly deepen our fundamental understanding of complex chemical reactions occurring at the liquid–solid interface.

AUTHOR INFORMATION

Corresponding Author

*Fax: + 86-551-3600437; e-mail: huangwx@ustc.edu.cn.

ACKNOWLEDGMENT

This work was financially supported by National Natural Science Foundation of China (grant 21173204), the solar energy project of Chinese Academy of Sciences, the Ministry of Science and Technology of China (2010CB923302), the Fundamental Research Funds for the Central Universities, and the MPG-CAS partner group.

REFERENCES

- (1) Gou, L. F.; Murphy, C. J. *Nano Lett.* **2003**, *3*, 231.
- (2) Li, X. D.; Gao, H. S.; Murphy, C. J.; Gou, L. F. *Nano Lett.* **2004**, *4*, 1903.
- (3) Kuo, C. H.; Chen, C. H.; Huang, M. H. *Adv. Funct. Mater.* **2007**, *17*, 3773.
- (4) Kuo, C. H.; Huang, M. H. *J. Phys. Chem. C* **2008**, *112*, 18355.
- (5) Zhang, D. F.; Zhang, H.; Guo, L.; Zheng, K.; Han, X. D.; Zhang, Z. *J. Mater. Chem.* **2009**, *19*, 5220.
- (6) Liang, X. D.; Gao, L.; Yang, S. W.; Sun, J. *Adv. Mater.* **2009**, *21*, 2068.
- (7) Yao, K. X.; Yin, X. M.; Wang, T. H.; Zeng, H. C. *J. Am. Chem. Soc.* **2010**, *132*, 6131.
- (8) Kuo, C. H.; Huang, M. H. *J. Am. Chem. Soc.* **2008**, *130*, 12815.
- (9) Zhang, Y.; Deng, B.; Zhang, T. R.; Gao, D. M.; Xu, A. W. *J. Phys. Chem. C* **2010**, *114*, 5073.
- (10) Wang, W. Z.; Wang, G. H.; Wang, X. S.; Zhan, Y. J.; Liu, Y. K.; Zheng, C. L. *Adv. Mater.* **2002**, *14*, 67.
- (11) Hong, X.; Wang, G.; Zhu, W.; Shen, X.; Wang, Y. *J. Phys. Chem. C* **2009**, *113*, 14172.
- (12) Singh, D. P.; Neti, N. R.; Sinha, A. S. K.; Srivastava, O. N. *J. Phys. Chem. C* **2007**, *111*, 1638.
- (13) Tan, Y. W.; Xue, X. Y.; Peng, Q.; Zhao, H.; Wang, T. H.; Li, Y. D. *Nano Lett.* **2007**, *7*, 3723.
- (14) Kuo, C. H.; Hua, T. E.; Huang, M. H. *J. Am. Chem. Soc.* **2009**, *131*, 17871.
- (15) Sui, Y. M.; Fu, W. Y.; Zeng, Y.; Yang, H. B.; Zhang, Y. Y.; Chen, H.; Li, Y. X.; Li, M. H.; Zou, G. T. *Angew. Chem., Int. Ed.* **2010**, *49*, 4282.
- (16) Lu, C. H.; Qi, L. M.; Yang, J. H.; Wang, X. Y.; Zhang, D. Y.; Xie, J. L.; Ma, J. M. *Adv. Mater.* **2005**, *17*, 2562.
- (17) Chang, Y.; Zeng, H. C. *Cryst. Growth Des.* **2004**, *4*, 273.
- (18) Chang, Y.; Teo, J. J.; Zeng, H. C. *Langmuir* **2005**, *21*, 1074.
- (19) Teo, J. J.; Chang, Y.; Zeng, H. C. *Langmuir* **2006**, *22*, 7369.
- (20) Ho, J. Y.; Huang, M. H. *J. Phys. Chem. C* **2009**, *113*, 14159.
- (21) Park, J. C.; Kim, J.; Kwon, H.; Song, H. *Adv. Mater.* **2009**, *21*, 803.
- (22) Wang, Z. Y.; Luan, D. Y.; Li, C. M.; Su, F. B.; Madhavi, S.; Boey, F. Y. C.; Lou, X. W. *J. Am. Chem. Soc.* **2010**, *132*, 16271.
- (23) Kuo, C. H.; Chu, Y. T.; Song, Y. F.; Huang, M. H. *Adv. Funct. Mater.* **2011**, *21*, 792.
- (24) Wen, X. G.; Zhang, W. X.; Yang, S. H. *Nano Lett.* **2002**, *2*, 1397.
- (25) Siegfried, M. J.; Choi, K. S. *Adv. Mater.* **2004**, *16*, 1743.
- (26) Siegfried, M. J.; Choi, K. S. *Angew. Chem., Int. Ed.* **2005**, *44*, 3218.
- (27) Siegfried, M. J.; Choi, K. S. *J. Am. Chem. Soc.* **2006**, *128*, 10356.
- (28) Bao, H. Z.; Zhang, W. H.; Shang, D. L.; Hua, Q.; Ma, Y. S.; Jiang, Z. Q.; Yang, J. L.; Huang, W. X. *J. Phys. Chem. C* **2010**, *114*, 6676.
- (29) Hua, Q.; Shang, D. L.; Zhang, W. H.; Chen, K.; Chang, S. J.; Ma, Y. S.; Jiang, Z. Q.; Yang, J. L.; Huang, W. X. *Langmuir* **2011**, *27*, 665.